International Micro Air Vehicle Conference and Flight Competition (IMAV2013)
17-20 September 2013, Toulouse, France

Near-Hover Flapping Wing MAV Aerodynamic Modelling - a linear model approach

J.V. Caetano[1,2] *, J. Verboom[1], C.C. de Visser[1], G.C.H.E. de Croon[1], B.D.W. Remes[1], C. de Wagter[1] and M. Mulder[1]

[1] Faculty of Aerospace Engineering, Delft University of Technology, The Netherlands
[2] Portuguese Air Force Research Center, Air Force Academy, Sintra, Portugal

Abstract

Flapping Wing Micro Air Vehicles typically have to be controlled actively in order to fly autonomously. Such active control benefits significantly from a model relating the flapper's state and control actions to the resulting forces and moments. This article presents the first results on system identification of a 17g ornithopter, the Delfly II. In particular, the Delfly II was programmed to perform specific flight manoeuvres in a high-fidelity sub-millimetre resolution external tracking system flight arena. The states were reconstructed and used to calculate the aerodynamic forces and moments that acted on the Delfly, under the assumptions of a rigid body and constant inertia properties, using general aircraft equations of motion. These forces and moments were used to identify parameters of a linear model around a trimmed hover condition. Two linear models are devised and compared: (1) a *full model* that incorporated state variables that were reconstructed from the tracking system, and (2) a *reduced model* that only included state variables that can be determined from onboard sensors. Using the linear time-invariant models it has been possible to estimate the aerodynamic forces with a very good approximation. However, neither the full nor the reduced models reveal to be able to estimate the aerodynamic moments as well as they do for the aerodynamic forces. The results point to the possibility of linear model use to control the Delfly in close-to-hover regime in closed loop.

1 Introduction

Flapping Wing Micro Air Vehicles (FWMAVs) pose many challenges, ranging from the understanding of their unsteady aerodynamics to designing the hardware. One of the greatest challenges is to achieve autonomous flight with ornithopters. Especially for nano FWMAVs, where flapping is believed to yield most advantages [1, 12, 14, 21], the small size and mass heavily restrict the possible sensors and processing onboard. At total take-off weights of only a few grams, attitude and flight control are still active areas of research [18, 26]. In this respect, a distinction has to be made between tailless and tailed designs.

Tailless designs offer the promise of performing highly dynamic manoeuvres as observed in small insects, such as bees and flies. However, these designs require active stabilization, as they are passively unstable. Although there is a considerable body of work on this type of FWMAV, only two such systems have shown actual flight ability: the Nano Hummingbird [18] and the Robobee [20]. The Nano Hummingbird utilizes onboard gyrometers and processing to perform onboard closed loop control on yaw, pitch and roll rates, positions of the yaw, pitch and roll servos, and the wing flapping frequency.

*Corresponding Author: j.v.caetano@tudelft.nl

Without human pilot input, the FWMAV performs autonomous attitude control on the basis of tuned control gains. The Robobee is extremely small and hence does not yet contain a power source, sensors, or processing onboard. It is able to hover and perform flight manoeuvres on the basis of a state estimate provided by external cameras. The control strategy for the attitude is based on a kinematic model and a corresponding Lyapunov function, resulting in a PD-like controller. The altitude and position are controlled with PD-controllers.

Tailed designs do not necessarily require active stabilization, because the tail acts as a natural damper. The centre of gravity can be placed such that close-to-hover flight becomes passively stable. Example studies using this set-up include [3, 8]. The advantage of this set-up is that research on such systems can focus on higher-level flight tasks such as altitude control [2, 10] or obstacle avoidance [9, 10]. A disadvantage of this set-up is that tailed FWMAVs are more sensitive to external perturbations. Moreover, it is very hard to maintain this stable configuration throughout the entire flight envelope without significant changes in, for instance, its centre of gravity. For this reason, active control is still necessary to enlarge the flight envelope, and to reject disturbances.

The previous approaches rely on manually tuned PID-controllers for the control of attitude and position. A model-based (nonlinear) control approach such as for example nonlinear dynamic inversion [24] could provide high performance control of the FWMAV over its entire flight envelope without the requirement for gain scheduling. The main reason behind the current absence of model-based control is the difficulty of designing a reliable model for FWMAVs. The principal difficulty derives from the unsteady aerodynamics [13] associated with flapping wing flight. Furthermore the flapping of the wings complicates the model description as their added inertia effects contribute to the dynamics [23] of the ornithopter. A complete modelling approach typically results [5, 23] in a complex nonlinear time-variant multi-body representation of the ornithopter. With the current state of technology it is not feasible to use such a model onboard for model-based control.

Aircraft system identification techniques have been applied before to a two wing ornithopter, with considerable success [17, 16]. However, this approach did not cover neither manoeuvre input design nor automated control over the inputs. More recently Caetano et al. have been able to program a FWMAV to perform automatic manoeuvres for system identification purposes [7] and calculate the aerodynamic forces and moments that act of the flapper, using flight path reconstruction and general aircraft equations of motion [6].

The **main contribution** of this article is centred around the development of computationally inexpensive linear model for the onboard control of the Delfly II FWMAV, which lead to the development of linear time-invariant aerodynamic models of the flapper that are valid for stable flight conditions. In particular, a high-fidelity sub-millimetre resolution external tracking system was used to directly measure the position and attitude of the Delfly II. The flight states were then reconstructed and used to calculate the aerodynamic forces and moments that acted on the flapper, under the assumptions of a rigid body and constant inertia properties (Section 2). Two linear models were devised and compared: (1) a *full model* that incorporates state variables reconstructed from the tracking system, and (2) a *reduced model* that only includes state variables that may be measured or calculated directly from the existing onboard sensors (Section 3). The quality of the results of these models if presented in Section 3.2. The final conclusions are drawn in Section 4.

2 System Overview

The present section describes the systems that were used for the flight tests and the respective data processing.

2.1 Delfly II Micro Air Vehicle

The Delfly II [11] is a bio-inspired ornithopter, configured with 4 flapping wings and an inverted "T" tail. It weighs only 17g and is capable of performing hovered flight as well as transition to a maximum forward flight speed of 5m/s and vice-versa. The Delfly that was used in the flight tests was equipped with a Radio Control (RC) receiver for manual operation and a programmable autopilot that is capable of performing stable automatic flight at a trimmed configuration. A full description of the Delfly can be found in [7] and [8].

2.2 Experimental Setup

The flight tests were conducted at the United States Research Laboratory Micro Air Vehicles Integration and Application Institute flight test chamber, that is equipped with a tracking system capable of recording the position of small reflective markers at 200Hz. In order to track the Delfly's position, eight markers were placed on the flappers' structure, as presented in Figure 1. In order to capture the full dynamic response of the Delfly over several dynamic frequencies, a set of in-flight longitudinal (elevator) inputs was designed and pre-programmed into the autopilot. This way the inputs were performed thoroughly by the autopilot with, assuring its constant duration and flight regime, that ranged from -0.25m/s to 1m/s ground speed. The elevator inputs were designed as steps, doublets and triplets with a reference time of $\frac{1}{3}$ of a second. More considerations about the markers' positions and the manoeuvre input design are presented in [7] and [6].

3 System Identification Framework

This section presents the system identification framework that was used to go from the tracking system data to the linear models for the aerodynamic forces and moments.

3.1 Flight Path Reconstruction

The first step in the system identification framework is the reconstruction of the Delfly states from the recorded position data in time. This process is called flight path reconstruction [22] and aims to reconstruct states that cannot be measured directly, such as the angle of attack, or to refine the accuracy of sensor measured states.

3.1.1 Reference Frames

In order to obtain the Delfly's states, each of the markers' coordinates has to be described in the Delfly's body frame. For the sake of simplicity, the tracking system's reference frame will be addressed as being the inertial frame. Hence, the inertial (subscript I) frame's z_I axis is vertical and positive up, and x_I and y_I axes are horizontal and form a right-handed orthonormal frame with z_I. The body reference frame (subscript b) was defined using an intermediate "marker" reference frame, as the markers were placed on top of the body structure and not *in* the body structure. The $\overrightarrow{x_b}$ axis is positive forward; the $\overrightarrow{z_b}$ was defined by the cross product of the unit vector of $\overrightarrow{x_b}$ with the unit vector that is defined by the left-to-right wing marker vector ($\overrightarrow{W_{LR}}$), thus $\overrightarrow{z_b} = normalized(\overrightarrow{i_b} \times \overrightarrow{W_{LR}})$. The $\overrightarrow{y_b}$ axis was then defined by the cross product of $\overrightarrow{z_b} \times \overrightarrow{x_b}$. The origin of the body frame is at the Delfly's Centre of Gravity (CG). Figure 2 presents both the inertial ($\overrightarrow{x_I}, \overrightarrow{y_I}, \overrightarrow{z_I}$) and body frames ($\overrightarrow{x_b}, \overrightarrow{y_b}, \overrightarrow{z_b}$).

The rotation matrices between the frames can be devised by using a direct cosine matrix. Eq. 1 represents the rotation matrix from the inertial to the body frame, in the way that a vector can be

Figure 1: Markers' positions on the Delfly.

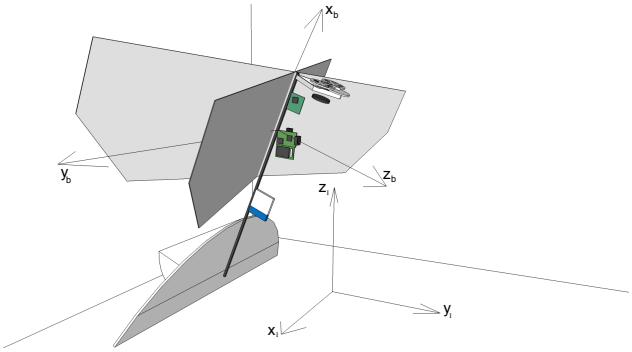

Figure 2: Inertial and body reference frames

calculated in the body frame by multiplying the rotation matrix Rot_{bI} with that vector's coordinates written in the inertial frame.

The Euler angles can be determined for each time step, by corresponding the, commonly called, 321 rotation matrix [4] to the markers coordinates in the inertial frame. The 321 rotation follows the *yaw* $(\psi) \longrightarrow$ *pitch* $(\theta) \longrightarrow$ *roll* (ϕ) sequence. One can easily obtain Rot_{bI} as a function of (ϕ, θ, ψ) by multiplying $Rot(\phi)Rot(\theta)Rot(\psi)$. The result is presented in Eq. 2. Hence, the (ψ, θ, ϕ) angles can be determined by relating the entries in Eqs. 1 and 2.

$$Rot_{bI} = \begin{bmatrix} i_{b_x} & i_{b_y} & i_{b_z} \\ j_{b_x} & j_{b_y} & j_{b_z} \\ k_{b_x} & k_{b_y} & k_{b_z} \end{bmatrix} \tag{1}$$

$$Rot_{bI} = \begin{bmatrix} \cos\theta\cos\psi & \cos\theta\sin\psi & -\sin\theta \\ \sin\phi\sin\theta\cos\psi - \cos\phi\sin\psi & \cos\phi\cos\psi + \sin\phi\sin\theta\sin\psi & \sin\phi\cos\theta \\ \sin\phi\sin\psi + \cos\phi\sin\theta\cos\psi & \sin\phi\cos\psi - \cos\phi\sin\theta\sin\psi & \cos\phi\cos\theta \end{bmatrix} \tag{2}$$

3.1.2 State Reconstruction

The Euler definition is limited to specific intervals [4] – for example, the θ angle is only defined in the interval $[-\frac{\pi}{2}; \frac{\pi}{2}]$. For the Delfly case, in a near-hover configuration, an elevator input can induce the transition to an inverted flight regime, where $\overrightarrow{z_b}$ is pointing upwards. In this situation, the ψ and ϕ have a sudden variation of 180°, as presented in Figure 5. In order to keep the Euler relations to be used in the general aircraft equations of motion (EOM) [15, 6], the Euler angles were converted to attitude angles ψ_y (yaw), θ_p (pitch) and ϕ_r (roll), as if these were measured on-board. This allows the dynamic equations to be defined over the ±90° pitch angle range and still remain in the same general form, not needing alternative formulations in terms of, e.g., quaternions. This way, angular rates (*p, q, r*) were obtained using Eq. 3. The linear velocities and accelerations, as well as the body angular accelerations ($\dot{p}$, $\dot{q}$, $\dot{r}$) were obtained by differentiating the markers positions and body rates, respectively, with respect to time. Table 1 presents all the states that were computed – they follow the commonly accepted definition in aeronautical engineering [15].

$$\begin{bmatrix} p \\ q \\ r \end{bmatrix} = \begin{bmatrix} 1 & 0 & -sin\theta_p \\ 0 & cos\phi_r & sin\phi_r cos\theta_p \\ 0 & -sin\phi_r & cos\phi_y cos\theta_p \end{bmatrix} \begin{bmatrix} \dot{\phi_y} \\ \dot{\theta_p} \\ \dot{\psi_r} \end{bmatrix} \tag{3}$$

Euler Angles	**Attitude Angles**	**Velocities**	**Accelerations**	**Angular Body Rates**	**Angular Body Accelerations**	**Aerodynamic Angles**	**Inputs**
ϕ	ϕ_r roll	u	$\dot{u}$	p	$\dot{p}$	α	δ_f (flap.freq.)
θ	θ_p pitch	v	$\dot{v}$	q	$\dot{q}$	β	δ_e (elevator)
ψ	ψ_y yaw	w	$\dot{w}$	r	$\dot{r}$	——	δ_r (rudder)
——	——	V	——	——	——	——	——

Table 1: Reconstructed states, using the flight data and respective control surface inputs.

Some of the reconstructed states are presented here for a near-hover elevator doublet input manoeuvre. In order to decrease the influence of the high oscillatory modes induced by the flapping frequency (comprehended between 12Hz and 13Hz for the present test case), the states were filtered using a 3^{rd} order zero-phase lag Butterworth low-pass filter, with cut-off frequency of 10Hz - data processing also revealed that neglecting the information of the fast high order harmonics just above the flapping frequency improves for the forces and moments estimation. This technique is also applied onboard, when reading from the inertial measurement unit.

Figures 3 to 6 present a part of one of the flight tests, zoomed around the doublet input on the elevator, where it is possible to observe the somewhat constant states prior to the input, as well as the Delfly's behaviour until the oscillatory movement is fully dampened. The elvator input had a 2/3 of a second, with each commanded deflection lasting 1/3 of a second. The abscissa axes are defined in seconds. In these Figures the blue lines represent the full dynamic oscillatory behaviour of the states without any filtering; the red lines represent the filtered states; *and* the green line in Figure 5 represents the attitude angles, presented in Table 1.

It is possible to follow the manoeuvre by observing Figures 3 and 4. The input starts at second 5.85 of the flight test. The rudder oscillation (Figure 3) during the longitudinal manoeuvre is related to the tail's rotation and bending, as no input over the rudder was performed by the autopilot. Figure 6presents the angle of attack (top) and side slip angle (bottom). The velocity component u (in Figure 4) decreases to a negative value as the Delfly loses lift and height. The oscillation in w is due to the pitch manoeuvre – when w goes to negative means the Delfly is flying in the opposite direction, in inverted flight. As expected, v does not suffer considerable variations during the longitudinal manoeuvre. The velocity variation between seconds 6 and 7 in Figure 4 corresponds to the inverted flight, where the Delfly is flying "belly up". The inverted flight can be better seen in Figure 5, by following the pitch angle on the middle graph (depicted in green), while it surpasses the 90° value.

3.2 Aerodynamic Model Identification

The second step in the system identification framework is aerodynamic model identification. The aim of aerodynamic model identification is to create a model that relates control actions to resulting aerodynamic forces and moments. The resulting aerodynamic models can then be used in model-based flight control systems.

3.2.1 Initial Assumptions

Creating accurate *full flight envelope* aerodynamic models of aircraft is a highly challenging task, especially when the aircraft is subject to significant nonlinear aerodynamics. However, if we focus on

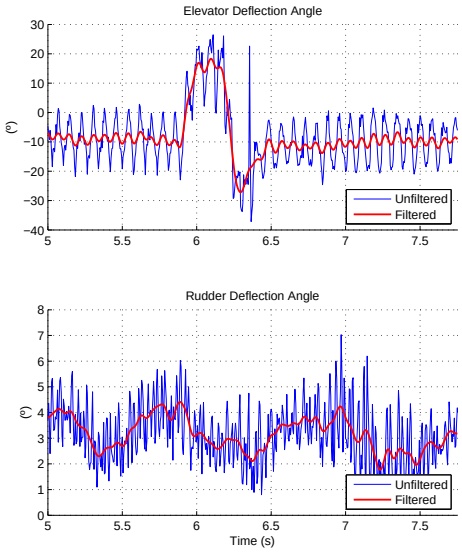

Figure 3: Elevator and rudder deflection angles, defined as positive up and right, respectively.

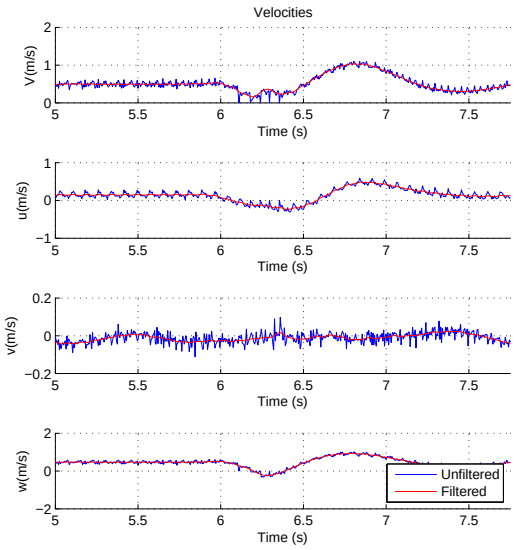

Figure 4: Body velocities in m/s. V corresponds to the free stream airspeed, decomposed in u, v and w for each of the body axes $(\overrightarrow{i_b}, \overrightarrow{j_b}, \overrightarrow{k_b})$.

small excitations around a stationary (trim) position, the nonlinear aerodynamics can be approximated with linear models [19]. In this work, we assume that Delfly is flying in a stationary condition and that the excitations around this condition are small. Under these assumptions, the linear modelling approach is valid.
Additionally, the dynamics of the Delfly are assumed to be described by the Newton-Euler equations of motion found in [19] or [6]. The assumptions involved are (1) rigid body kinematics; (2) no flapping (the flapping is then modelled as a thrust force); (3) constant mass and no inertia changes due to flapping or bending; (4) flat Earth; (5) no wind.

3.2.2 Model Structure Selection and Parameter Estimation

Several linear model structures of the form $X = X_{0_s} + \sum_{s=1}^{n} X_s.S$ were devised using a linear states' relation. Here the left-hand side term X represents the forces and moments obtained from the Newton-Euler equations of motion [4, 6]; the first term on the right-hand side, X_{0_s}, is the affine coefficient; S represents a state and X_S the state's coefficient or parameter for a given force or moment X. The flight test data was divided into *identification* and *validation* sets. The identification set is used to estimate the aerodynamic parameters; the validation set is used to verify if the estimated model is able to represent the aerodynamic forces and moments.

Under the previously mentioned premise, the *full* model was devised in the way that each of the aerodynamic forces (X, Y, Z) and moments (L, M, N) are a linear function of the following states (S): ϕ_r, θ_r, ψ_r, u, v, w, p, q, r, α, β, δ_f, δ_e, δ_r.

The *reduced* model presented in Eq. 4 was devised in order to test the states estimation capabilities of a simple and computational inexpensive linear model, that uses the states that can be measured onboard.

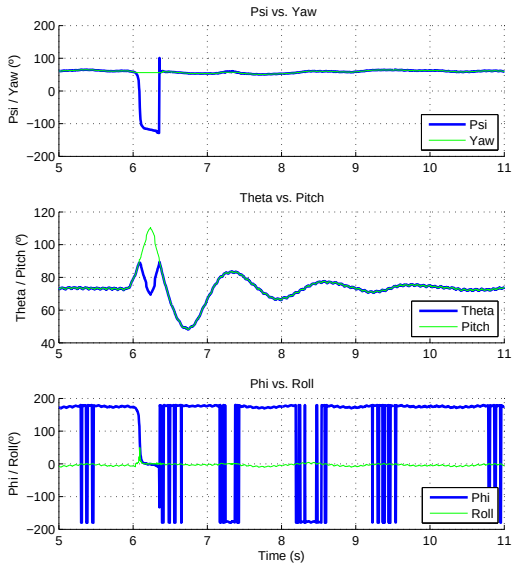

Figure 5: Euler angles (blue) and attitude angles (green).

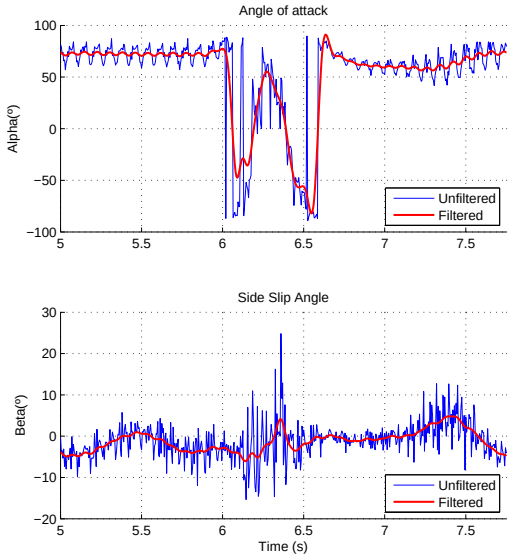

Figure 6: Attack (top) and side slip angles (bottom).

$$
\begin{aligned}
X &= X_0 + X_q q + X_\theta \theta + X_{\delta_e}\delta_e + X_{\delta_f}\delta_f \\
Y &= Y_0 + Y_p p + Y_\phi \phi + Y_{\delta_r}\delta_r + Y_{\delta_f}\delta_f \\
Z &= Z_0 + Z_q q + Z_\theta \theta + Z_{\delta_e}\delta_e + Z_{\delta_f}\delta_f \\
L &= L_0 + L_\theta \theta + L_{\delta_r}\delta_r + L_{\delta_f}\delta_f \\
M &= M_0 + M_\theta \theta + M_{\delta_e}\delta_e + M_{\delta_f}\delta_f \\
N &= N_0 + N_\theta \theta + N_{\delta_r}\delta_r + N_{\delta_f}\delta_f
\end{aligned}
\tag{4}
$$

An ordinary least squares estimator was used to estimate the parameters in the linear models. As an example, to estimate the parameters in the equation for X in Eq. 4 we get:

$$
\begin{bmatrix} \hat{X_0} \\ \hat{X_q} \\ \hat{X_\theta} \\ \hat{X_{\delta_e}} \\ \hat{X_{\delta_f}} \end{bmatrix} = (\mathbf{R}^\top \mathbf{R})^{-1} R^\top X \quad (5) \qquad \text{with} \qquad \mathbf{R} = \begin{bmatrix} 1 & q(1) & \theta(1) & \delta_e(1) & \delta_f(1) \\ 1 & q(2) & \theta(2) & \delta_e(2) & \delta_f(2) \\ \vdots & \vdots & \vdots & \vdots & \\ 1 & q(N) & \theta(N) & \delta_e(N) & \delta_f(N) \end{bmatrix} \tag{6}
$$

with the regression matrix $\mathbf{R}$ containing a total of N observations.

3.2.3 Model Validation

This subsection presents the aerodynamic forces and moments' estimation results for both the full and the reduced models.

The states that were used to compute the aerodynamic forces and moments were filtered (as mentioned in section 3.1.2). This is coherent with the current PID control solutions that have been previously implemented on the Delfly, as the high order fast oscillations are filtered from the accelerometer and gyroscope information, for controllability purposes.

A set of different near-hover condition flight tests, with dissimilar elevator inputs was evaluated in this routine. The results show that the models are able to estimate the aerodynamic forces with great approximation. The moments, however, cannot be estimated as well as the forces but are still able follow the calculated moments (from the EOM) around the manoeuvres.

The results are presented for the same test and for the same part of the flight as presented in Figures 3 to 6. Hence, Figures 7 and 8 present the graphical evolution of the filtered forces and moments respectively. These Figures present the final results of the *validation* part of the system identification. The blue lines represent forces and moments calculated using the aircraft EOM; the red lines depict the full linear model's evolution; whereas the green lines describe the reduced model's behaviour.

Both models are able to follow all aerodynamic forces with a good approximation capability (Figure 7). The variation in the results for the peak in the X force result from the fact that the X force that was computed from the EOM is highly affected by the velocity component in w, which drops to negative values when the Delfly flies inverted. Both models are able to estimate the Z force with a very good performance. The Y force does not vary considerably in the (longitudinal) manoeuvre, as no rudder input was present. Despite some punctual differences, the Y force is also well estimated by both models.

None of the models is able to completely follow the aerodynamic moments' evolution (Figure 8). For the case shown here, the most important moment (M) is also the best estimated one. However, the *full* model is not able to completely follow the moments around the manoeuvre and the *reduced* model presents a slight phase lag on the results. The L and N moments are not well estimated by none of the models for longitudinal manoeuvres. Nevertheless, these are able to follow the computed (EOM) L and N moments for lateral inputs on the rudder, where it is noticeable a coupling between all 3 moments – a rudder deflection of the Delfly induces a nose-down manoeuvre, due to the vertical arm of the rudder, with respect to the flappers centre of gravity.

The estimated aerodynamic moments present a cycle averaged behaviour similar to the ones computed out of the EOM, pointing to a possible application for onboard control, using online filtering of the states or a more refined linear model.

A quantitative measurement of the performance of the model is given by calculating Pearson's correlation coefficient between each of the model's estimations and the forces and moments that were computed from the EOM. The correlation coefficient captures how two signals vary with respect to their means and is defined as $\rho = \frac{\mathrm{cov}(X_{EOM}, X_{estim})}{\sigma(X_{EOM})\sigma(X_{estim})}$. The best performance would be the highest correlation of $\rho = 1$, while completely decorrelated signals would give $\rho = 0$. Table 2 shows the correlation coefficients for the full model and reduced model. It can be seen that the forces X, Y, and Z are well estimated with $\rho \in [0.85, 0.99]$. The moment predictions are still reasonably correlated for the *full* model ($\rho \in [0.39, 0.62]$), but only slightly correlated for the *reduced* model $\rho \in [0.14, 0.43]$.

Pearson's Correlation Coefficient

Forces and Moments	**X**	**Y**	**Z**	**L**	**M**	**N**
Full Model	0.88	0.97	0.99	0.39	0.62	0.46
Reduced Model	0.85	0.95	0.99	0.14	0.43	0.21

Table 2: Pearson's Correlation Coefficient between each of the linear models and the calculated forces and moments.

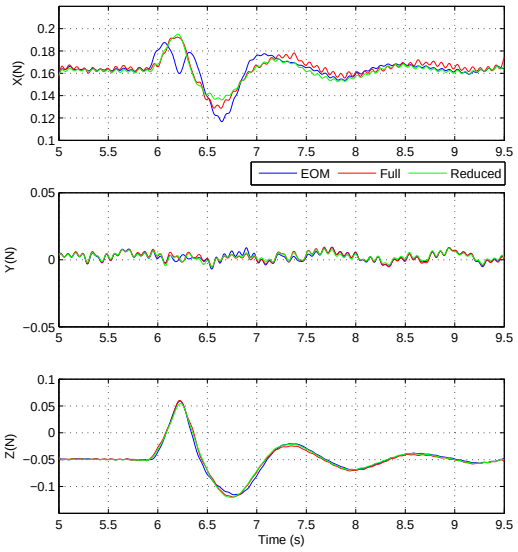

Figure 7: Calculated (blue) and estimated forces for both the full (red) and reduced (green) models, around the elevator input manoeuvre.

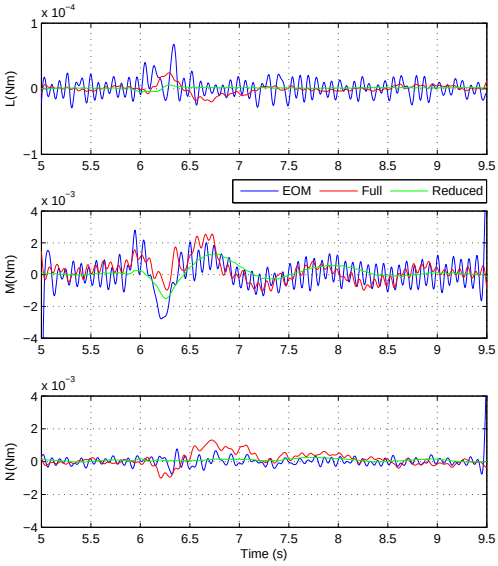

Figure 8: Calculated (blue) and estimated moments for both the full (red) and reduced (green) models, around the elevator input manoeuvre.

4 Conclusion

Two Delfly models were devised with the intention of achieving a linear time-invariant model description of the Delfly's aerodynamics. The linear models were designed from a control-driven perspective with the goal of using these models for onboard control and flight simulation purposes. Both the *full* and the *reduced* models were able to estimate the aerodynamic forces and moments, with better results on the *full* model. As a simple approximation, the consistency of the results conclude that the forces are well enough estimated to make a both linear models applicable for flight simulation as well as for onboard flight control. The moment's estimation results point to a possible application of these results for onboard control, using sensor fusion, onboard cycle average filtering and attitude thresholds. Further analyses will be conducted to search for other models, as well as to extend the results to other flight regimes and implement a controller based on the models to assess the flappers controllability.

References

[1] S. Ansari, R. Zbikowski, and K. Knowles. Aerodynamic modelling of insect-like flapping flight for micro air vehicles. *Progress in Aerospace Sciences*, 42(2):129–172, 2006.

[2] S. Baek and R. Fearing. Flight forces and altitude regulation of 12 gram i-bird. In *IEEE RAS and EMBS International Conference on Biomedical Robotics and Biomechatronics (BioRob)*, pages 454–460, 2010.

[3] S. S. Baek. Autonomous ornithopter flight with sensor-based behavior. *Univ. California, Berkeley, Tech. Rep. UCB/EECS-2011-65*, 2011.

[4] H. Baruh. *Analytical Dynamics*. McGraw-Hill Higher Education, 1999.

[5] M. A. Bolender. Rigid multi-body equations-of-motion for flapping wing mavs using kanes equations. In *AIAA Guidance, Navigation, and Control Conference*, August 2009.

[6] J. Caetano, C. C. de Visser, B. Remes, C. de Wagter, and M. Mulder. Modeling a flappingwing mav: Flight path reconstruction of the delfly ii. AIAA, 2013.

[7] J. V. Caetano, C. C. de Visser, B. Remes, C. de Wagter, and M. Mulder. Controlled flight maneuvers of a flapping wing micro air vehicle: a step towards the delfly ii identification. In *AIAA Atmospheric Flight Mechanics Conference*, 2013.

[8] G. De Croon, K. De Clercq, R. Ruijsink, B. Remes, and C. De Wagter. Design, aerodynamics, and vision-based control of the delfly. *International Journal of Micro Air Vehicles*, 1(2):71–97, 2009.

[9] G. de Croon, E. de Weerdt, C. de Wagter, B. Remes, and R. Ruijsink. The appearance variation cue for obstacle avoidance. *IEEE Transactions on Robotics*, 28(2):529–534, 2012.

[10] G. de Croon, Groen, M., C. de Wagter, B. Remes, R. Ruijsink, and B. van Oudheusden. (accepted) design, aerodynamics, and autonomy of the delfly. *In Bioinspiration and Biomimetics*, 2012.

[11] Delfly Team. Delfly. www.delfly.nl, accessed on January 5th, 2013.

[12] M. Dickinson, F.-O. Lehmann, and S. Sane. Wing rotation and the aerodynamic basis of insect flight. *Science*, 284(5422):1954–1960, 1999.

[13] C. Ellington. The aerodynamics of hovering insect flight. i. the quasi-steady analysis. *Philosophical Transactions of the Royal Society of London. B, Biological Sciences*, 305(1122):1–15, 1984.

[14] C. Ellington, C. Berg, A. van den Willmott, and A. Thomas. Leading-edge vortices in insect flight. *Nature*, 384(19/26):626–630, 1996.

[15] B. Etkin and L. D. Reid. *Dynamics of Flight: Stability and Control*. Jonh Wiley & Sons, Inc., 3rd edition, 1996.

[16] J. Grauer, E. Ulrich, J. H. Jr., D. Pines, , and J. S. Humbert. Testing and system identification of an ornithopter in longitudinal flight. *Journal of Aircraft*, 48(2):660–667, March-April 2011.

[17] J. Grauer, E. Ulrich, J. H. Jr., D. Pines, and J. S. Humbert. System identification of an ornithopteraerodynamics model. AIAA, August 2010.

[18] M. Keennon, K. Klingebiel, H. Won, and A. Andriukov. Development of the nano hummingbird: A tailless flapping wing micro air vehicle. In *Proc. of 50th AIAA Aerospace Science Meeting, Nashville, TN, January*, pages 06–12, 2012.

[19] V. Klein and E. A. Morelli. *Aircraft System Identification: Theory And Practice*.

[20] K. Ma, P. Chirarattananon, S. Fuller, and R. Wood. Controlled flight of a biologically inspired, insect-scale robot. *Science*, 340(6132):603–607, 2013.

[21] V. Malolan, M. Dineshkumar, and V. Baskar. Design and development of flapping wing micro air vehicle. In *42nd AIAA Aerospace Sciences Meeting and Exhibit, 5 - 8 January, Reno, Nevada*, 2004.

[22] J. A. Mulder, Q. P. Chu, J. K. Sridhar, J. H. Breeman, and M. Laban. Non-linear aircraft flight path reconstruction review and new advances. *Progress in Aerospace Sciences*, 35:673–726, 1999.

[23] C. T. Orlowski and A. R. Girard. Modeling and simulation of nonlinear dynamics of flapping wing micro air vehicles. *AIAA journal*, 49(5):969–981, 2011.

[24] J. Reiner, G. J. Balas, and W. L. Garrard. Flight control using robust dynamic inversion and time-scale separation. *Automatica*, 32:1493–1504, 1996.

[25] H. E. Taha, M. R. Hajj, and A. H. Nayfeh. Flight dynamics and control of flapping-wing mavs: a review. *Nonlinear Dynamics*, 70:907–939, 2012.

[26] R. Wood. The first takeoff of a biologically-inspired at-scale robotic insect. *IEEE Tranactions on Robotics*, 24(2):341–347, 2008.